THE JOURNAL OF PHYSICAL CHEMISTRY A
A JOURNAL OF THE AMERICAN CHEMICAL SOCIETY

pubs.acs.org/JPCA Article

Theoretical Characterizations of TADF Materials: Roles of ΔG and the Singlet−Triplet Excited States Interconversion

Lu Wang, Qi Ou, Qian Peng,* and Zhigang Shuai*

Cite This: J. Phys. Chem. A 2021, 125, 1468−1475 Read Online

ACCESS | Metrics & More | Article Recommendations | Supporting Information

ABSTRACT: The thermally activated delayed fluorescence (TADF) phenomenon has attracted increasing attention because it can harvest 100% of the electro-pumped carriers to form singlet bound excited state for fluorescence. It is generally believed that the small energy gap between S_1 and T_1 (ΔE_{ST}) is essential for TADF to facilitate the reverse intersystem crossing (rISC). However, for a few donor−acceptor (D−A) organic compounds with small ΔE_{ST}, the TADF phenomenon is absent, indicating that ΔE_{ST} might not be a good molecular descriptor. Here, using our self-developed thermal vibration correlation function (TVCF) formalism in combination with quantum chemistry calculations, we revisit the key factors that dominate the TADF property for 11 D−A systems with small ΔE_{ST}. Based on our theoretical results in comparison to experiments, we conclude that the activation energy ΔG is a good molecular descriptor to characterize the TADF performance because a significantly better linear relationship is observed between ΔG and the rISC rate constant (k_{rISC}) compared to that between ΔE_{ST} and k_{rISC}. These findings provide deeper understanding of the TADF mechanism, shedding light on the molecular design of high-performance TADF materials.

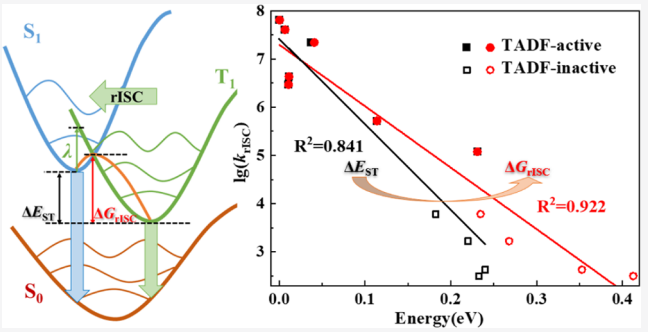

1. INTRODUCTION

Thermally activated delayed fluorescence (TADF) materials have attracted increasing attention for organic light-emitting diodes (OLEDs) because of their ability to harness all of the electrogenerated triplet and singlet excitons for fluorescence.[1−8] Deep understanding of the TADF mechanism and the establishment of good descriptors are very important for the molecular design of highly efficient TADF materials.[9−11] In the TADF process of organic molecules, the triplet exciton first goes uphill to the singlet excited state through reverse intersystem crossing (rISC) and then emits fluorescence. Therefore, the rISC process is key to the occurrence of the TADF phenomenon.

It is generally accepted that a heavy atom is required to provide large spin−orbit coupling (ξ) for mutual conversion between singlet and triplet states in metal complexes.[12] Adachi et al. claimed that the highly efficient spin conversion can take place without heavy atoms as long as a molecule possesses a small ΔE_{ST} and a nonvanishing small spin−orbit coupling (ξ) because the mixing coefficient between singlet and triplet states (c_{ST}) is inversely proportional to ΔE_{ST} by $c_{ST} \propto \xi/E_{ST}$.[1,13] Driven by this notification, researchers started to pursue ultrasmall ΔE_{ST} through designing a twisted donor−acceptor (D−A) molecular structure, which can produce space-separated highest occupied molecular orbital (HOMO) and lowest unoccupied molecular orbital (LUMO) to decrease the electronic exchange energy so that charge-transfer ^{1}CT and ^{3}CT states can be energetically degenerate.[14] ΔE_{ST} < 0.1 eV was once regarded as a necessary condition to generate TADF for organic compounds,[1] and TADF materials with almost zero energy gap were synthesized by the Adachi group.[15] However, ξ between two complete CT states (^{1}CT and ^{3}CT) is zero according to the El-Sayed rule, which would surely prevent the occurrence of rISC according to the rate formalism.[16] Through investigating the rISC rate constant as a function of energy gap at different temperatures of TADF molecule via the thermal vibration correlation function (TVCF) formalism,[17] Peng et al. proposed that the most efficient rISC process approximately appears at $\Delta E_{ST} = \lambda$ instead of $\Delta E_{ST} = 0$, in which the rISC rate is almost temperature-independent, namely, it can occur without thermal activation.[18] Samanta et al. have drawn the same conclusion that a sufficient reduction in ΔE_{ST} is not necessarily required for TADF compounds.[9] Through spectroscopic measurements, Adachi et al. also observed that compounds with similar ΔE_{ST} values exhibit different TADF properties, namely, some are TADF-active while others are TADF-inactive.[19,20] In addition, some declarations suggest that the involved intermediate local excitation (LE) states[19,21] or

Received: November 1, 2020
Revised: January 27, 2021
Published: February 15, 2021

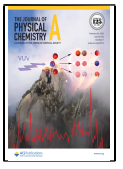

https://dx.doi.org/10.1021/acs.jpca.0c09767
J. Phys. Chem. A 2021, 125, 1468−1475

Scheme 1. Compounds Investigated in This Work, with Blue Indicating Donor Moieties and Red Denoting Acceptor Moieties

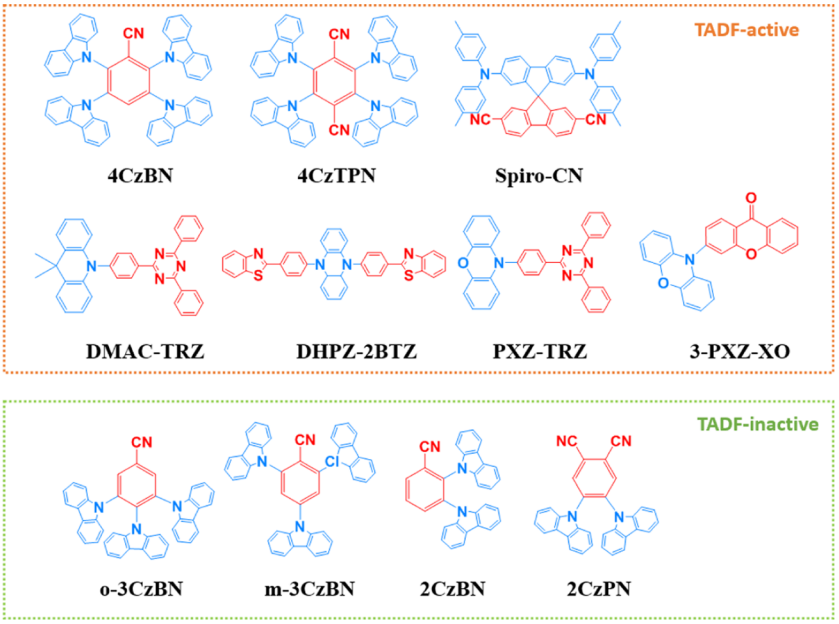

the Herzberg–Teller effect[22,23] induce significant spin–orbit coupling for an efficient rISC process between ^{1}CT and ^{3}CT states.

In this work, using our self-developed TVCF rate theory coupled with quantum chemistry calculations, we systematically investigated the structure–property relationship between singlet–triplet energy gap (ΔE_{ST}), reorganization energy (λ), activation energy (ΔG), and interconversion rates ($k_{ISC/rISC}$) between S_1 and T_1 for seven TADF-active and four TADF-inactive organic compounds with similar ΔE_{ST} (see Scheme 1).[1,15,24−27] Based on our theoretical results and the experimental facts, we conclude that activation energy ΔG is a good molecular descriptor to characterize the TADF performance because of a significantly better linear relationship between ΔG and $k_{ISC/rISC}$ compared to that between ΔE_{ST} and $k_{ISC/rISC}$. These findings provide deeper understanding of the TADF mechanism and open a novel design strategy to broaden the scope of high-performance organic TADF materials.

2. THEORETICAL MODEL AND METHODOLOGICAL APPROACHES

Based on Fermi's golden rule, second-order perturbation theory, and Born–Oppenheimer adiabatic approximation, the intersystem crossing rate constant is generally expressed as

$$k_{ISC} = \frac{2\pi}{\hbar}\sum_{v_i,v_f} P_{v_i}(T)\left|\hat{H}'_{v_f,v_i} + \sum_{v_n}\frac{\hat{H}'_{v_f,v_i}\hat{H}'_{v_n,v_i}}{E_{i,v_i} - E_{f,v_f}}\right|^2 \delta(E_{i,v_i} - E_{f,v_f}) \quad (1)$$

where $\hbar$ is Planck's constant; P_{v_i} is the Boltzmann distribution of the vibration manifolds in the initial electronic state; v_i,v_n, and v_f are the vibrational quantum numbers of the initial, intermediate, and final electronic states, respectively; and H' denotes the interaction between two different Born–Oppenheimer states, consisting of two contributions

$$\hat{H}'\Psi_{i,v_i} = \hat{H}^{BO}\Phi_i(\mathbf{r};\mathbf{Q})\Theta_{v_i}(\mathbf{Q}) + \hat{H}^{SO}\Phi_i(\mathbf{r};\mathbf{Q})\Theta_{v_i}(\mathbf{Q}) \quad (2)$$

where the first term corresponds to the nonadiabatic coupling and the second term corresponds to spin–orbit coupling.

Applying the Franck–Condon principle and the TVCF method, we rewrite eq 1 as

$$k_{ISC} = \frac{1}{\hbar^2}(k^{(0)}_{f\leftarrow i} + k^{(1)}_{f\leftarrow i} + k^{(2)}_{f\leftarrow i}) \quad (3)$$

$$k^{(0)}_{f\leftarrow i} \equiv \int_{-\infty}^{\infty} dt e^{i\omega_{if}t}|\xi_{if}|^2\rho^{(0)}_{fi}(t,T) \quad (4)$$

$$k^{(1)}_{f\leftarrow i} \equiv \mathrm{Re}\left[2\int_{-\infty}^{\infty} dt e^{i\omega_{if}t}\sum_k \xi_{if}T_{if,k}\rho^{(1)}_{fi,k}(t,T)\right] \quad (5)$$

$$k^{(2)}_{f\leftarrow i} \equiv \int_{-\infty}^{\infty} dt e^{i\omega_{if}t}\sum_{k,l} T_{if,k}T_{fi,l}\rho^{(2)}_{fi,kl}(t,T) \quad (6)$$

$$T_{if,k} \equiv \sum_n\left(\frac{\xi_{in}R_{nf,k}}{\Delta E_{nf}} + \frac{R_{in,k}\xi_{nf}}{\Delta E_{in}}\right) \quad (7)$$

Here, $R_{if,k} = \langle\Phi_f|\hat{P}_{fk}|\Phi_i\rangle$ is the nonadiabatic electronic coupling between two electronic states and $\rho^{(0)}_{fi}(t,T)$, $\rho^{(1)}_{fi,k}(t,T)$, and $\rho^{(2)}_{fi,kl}(t,T)$ are three thermal vibration correlation functions, whose analytical solution can be found in ref 17. The ISC rate formula can tackle the case in which the ISC process effectively occurs with the help of intermediate states. A similar expression can be obtained for rISC rate constant with different initial and final electronic states compared to the corresponding ISC rate constant. It should be noted that $\Delta E_{if} = E_i - E_f$ is positive for the ISC process while negative for the rISC process. For the ISC process, $\Delta E_{if} = \Delta E_{ST}$; for the rISC process, $\Delta E_{if} = -\Delta E_{ST}$.

For the case of strong coupling, one can apply short-time approximation $\left(\exp(it\omega_k) = 1 + it\omega_k + \frac{(it\omega_k)^2}{2!} + ...\right)$ and high-temperature approximation ($kT/\hbar\omega_k \gg 1$) and neglect the first- and second-order terms. The ISC rate is then represented by the following Marcus–Levich equations[28]

https://dx.doi.org/10.1021/acs.jpca.0c09767
J. Phys. Chem. A 2021, 125, 1468−1475

$$k_{\mathrm{ISC/rISC}} = \frac{1}{\hbar}|\xi_{if}|^2\sqrt{\frac{\pi}{\lambda k_{\mathrm{B}}T}}\exp\left[-\frac{(\Delta E_{if}-\lambda)^2}{4\lambda k_{\mathrm{B}}T}\right] \quad (8)$$

From eq 8, it can be intuitively seen that (i) the intersystem crossing is induced by the spin−orbit coupling ξ_{if}. If ξ_{if} vanishes, the ISC or rISC is prohibited for two electronic states even with $E_{if} = 0$. In this work, we set ξ_{if} to be a constant of 0.5 cm^{-1} for the reason that ξ_{if} for all investigated compounds ranges from 0.003 to 1.746 cm^{-1} (see Table S3). (ii) The reorganization energy λ is also very important to tune the rate constant value, which can be evaluated by

$$\lambda = \sum_k \lambda_k \quad (9)$$

$$\lambda_k = S_k\hbar\omega_k = \frac{1}{2}\omega_k^2 D_k^2 \quad (10)$$

Here, ω_k, S_k, and λ_k are the frequency, Huang−Rhys factor, and reorganization energy of kth normal modes, respectively. In practice, we calculate λ at both S_1 and T_1 optimized structures and the average value of these two reorganization energies is substituted into eq 8.

Equation 8 intuitively depicts the relation between the ISC/rISC rate constant and the energy gap as well as the reorganization energy. We plot the potential energy surfaces of the S_0, S_1, and T_1 states with the nonradiative transitions in Figure 1a. It is easily seen that ΔE_{if} is always much larger than λ ($\Delta E_{if} \gg \lambda$) for the nonradiative decay processes back to the ground state, i.e., $S_1 \rightarrow S_0$ and $T_1 \rightarrow S_0$, while for the ISC process between S_1 and T_1, the values of λ and ΔE_{if} are comparable. The ISC/rISC rate constants as a function of ΔE_{if} are given in Figure 1b based on eq 8. From eq 8 and Figure 1b, $k_{\mathrm{ISC/rISC}}$ is maximized when $\Delta E_{if} = \lambda$. Figure 1b can be divided into two regions, i.e., normal region with $\Delta E_{if} < \lambda$ and inverted region with $\Delta E_{if} > \lambda$. As ΔE_{if} increases, the rate constant increases in the normal region while decreases in the inverted region. Owing to the fact that ΔE_{if} ranges between −0.5 and 0.5 eV, which is comparable to the value of λ, the rISC and ISC rates always span the two regions, which leads to a nonmonotonic relationship between the rate constant and energy gap. Thus, the energy gap law becomes invalid in a such case. This revises the conventional conception that the rate is infinitely increased when the energy gap is close to zero.

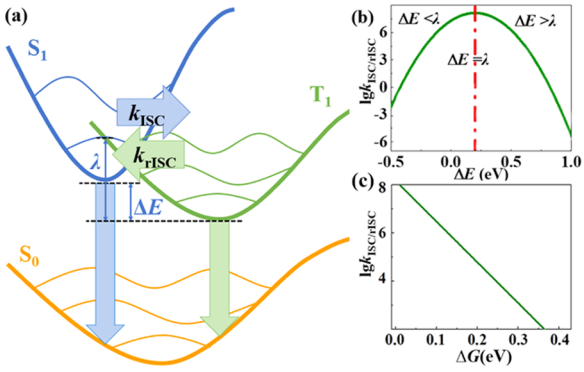

Figure 1. (a) Potential energy surfaces of the S_0, S_1, and T_1 states and the nonradiative transitions between states with energy gap (ΔE) and reorganization energy (λ). (b) ISC and rISC rate constants versus ΔE based on eq 8. (c) ISC and rISC rate constants versus ΔG based on eq 8. ξ_{if} is set to be 0.5 cm^{-1} in (b) and (c).

Equation 8 can be rewritten in an Arrhenius-like form as follows

$$k_{\mathrm{ISC/rISC}} = A\exp\left[-\frac{\Delta G}{RT}\right] \quad (11)$$

where

$$A = \frac{1}{\hbar}|\xi_{if}|^2\sqrt{\frac{\pi}{\lambda k_{\mathrm{B}}T}} \quad (12)$$

and

$$\Delta G = \frac{(\Delta E_{if}-\lambda)^2}{4\lambda} \quad (13)$$

Practically, we compute ΔG in two ways: the first one is based on eq 13, which is marked as ΔG_1; the second one is via a linear fitting between the logarithm of the computed TVCF rate constants versus the temperature (details in Part 8 of the Supporting Information), which is marked as ΔG_2. In this work, we demonstrate that ΔG is a more appropriate descriptor of TADF materials instead of ΔE_{ST} because it can take the vibration relaxation between S_1 and T_1, i.e., reorganization energy, into consideration. Note that thermal vibrational effect has been explicitly taken into account in ΔG_2 via TVCF, which should serve as a more sophisticated descriptor compared to ΔG_1. In Figure 1c, we plot rate constant as a function of ΔG. Clearly in Figure 1c, a linear relationship is observed between ΔG and $\log k$, i.e., the rate constant increases monotonically as ΔG decreases. Therefore, ΔG is theoretically a more convincing descriptor for ISC/rISC

Scheme 2. Schematic Graph for Molecular Design of Efficient TADF Materials

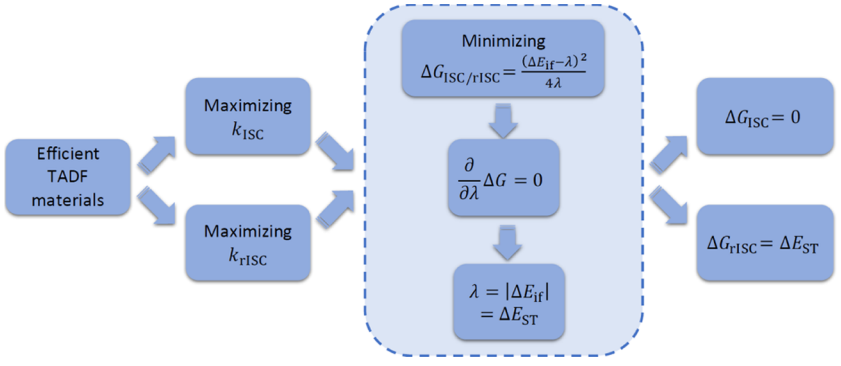

https://dx.doi.org/10.1021/acs.jpca.0c09767
J. Phys. Chem. A 2021, 125, 1468−1475

processes in TADF materials, as indicated in ref 18 as well as the Marcus theory.

Based on the aforementioned analysis, one needs to focus on the minimization of ΔG instead of E_{ST} for the molecular design of efficient TADF materials, as shown in Scheme 2. For both ISC and rISC processes, $\lambda = \Delta E_{ST}$ is required to get the maximum transition rate. For the ISC process under such condition, ΔG tends to zero, i.e., the ISC process becomes a barrierless process. For the rISC process, the minimum value of ΔG equals to ΔE_{ST}, i.e., ΔE_{ST} is the minimum of energy potential barrier for the rISC process. In other words, when the reorganization energy shares a similar value to the energy gap, the rate of rISC is directly determined by ΔE_{ST} since $\Delta G \approx \Delta E_{ST}$. However, when the value of λ differs from ΔE_{ST}, ΔG will deviate from ΔE_{ST}, leading to the fact that the TADF activity is no longer ΔE_{ST}-related. That is the reason why although several compounds investigated in this work have similar ΔE_{ST}, only part of them are TADF-active, which leads to a new direction of molecular design.

In this work, geometry optimizations and frequency analyses were performed by density functional theory (DFT) for S_0 and T_1, respectively, and time-dependent DFT (TDDFT) was performed for the S_1 state, under the CAM-B3LYP/6-31G* level. Here, we compare the T_1 geometry via unrestricted DFT (UDFT) and Tamm−Dancoff approximation (TDA) of *o*-3CzBN and 4CzTPN for test and found that the results are very similar. The root-mean-square displacement (RMSD) values of these two methods are 0.280 and 0.013 Å, respectively (Figure S7). And all of the optimized geometries can be found in Part 9 of the Supporting Information. The scale factors of frequencies are fitted to be 0.9495 (see Part 1 of the Supporting Information) under this calculation level.[29] The PBEα_0 method (TDA-PBEα_0/6-31+G*) is applied to get the excitation energies[30] (see Part 2 of the Supporting Information). All of the calculations took solvent (toluene) effect into consideration with the solvation model based on density (SMD).[31] These quantum chemistry calculations were performed in Gaussian 16.[32] The rate constants of ISC and rISC were computed by the TVCF approach in our home-built MOMAP package.[17,33−35] More computational details can be found in the Supporting Information.

3. RESULTS AND DISCUSSION

First, based on the computational model, we optimize the molecular geometries of S_0, S_1, and T_1 and get the excitation energy. The computational results of the emission energy (E_{emi}) and the energy gap ($\Delta E_{ST\text{-}00}$) after zero-point vibration energy correction (ΔE_{ZPVE}), $\Delta E_{ST\text{-}00} = \Delta E_{ST\text{-}ad} + \Delta E_{ZPVE}$, versus the experimental counterparts are plotted in Figure 2, while the explicit values can be found in Table S4. It is found that most of the data points lie close to the diagonal line in Figure 2, which reflects the fact that the calculated emission energy as well as the 0−0 energy gap ($\Delta E_{ST\text{-}00}$) are in good agreement with the experimental results. This proves the reliability of our applied electronic structure method. Note that rather large deviations are observed for $\Delta E_{ST\text{-}00}$ of 2-CzBN and *m*-3CzBN, and taking *m*-3CzBN as an example, the calculated excitation energy of S_1 (ΔE_{emi}) of *m*-3CzBN is 2.79 eV, well matching the experimental value of 2.90 eV with a small deviation of 0.11 eV. The calculated excitation energy of T_1 (ΔE_T) of *m*-3CzBN is 2.69 eV, in good agreement with the experimental value of 2.85 eV with a small deviation of 0.16 eV. But the resultant theoretical and experimental ΔE_{ST} values

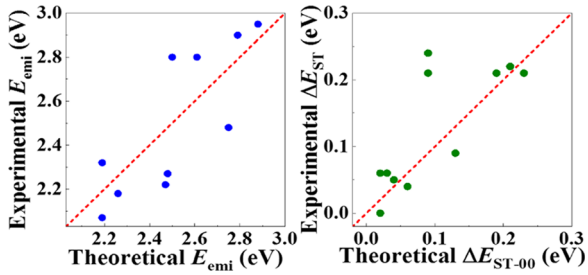

Figure 2. Comparison between theoretical (TDA-PBEα_0/6−31+G* with SMD) and experimental emission energies (left) and $\Delta E_{ST\text{-}00}$ (right).

are 0.09 eV and 0.24 eV, respectively, which lead to a large deviation of 0.15 eV. Because ΔE_{ST} is a small quantity, namely, 0.24 eV, the deviation of 0.15 eV is a large one. It is still a great challenge to obtain reasonable ΔE_{emi}, ΔE_T, and ΔE_{ST} simultaneously. Therefore, we compute the adiabatic energy gap ($\Delta E_{ST\text{-}ad}$) of these two molecules, which is applied in the following rate constant calculations, by subtracting the calculated ΔE_{ZPVE} from the experimental $\Delta E_{ST\text{-}00}$. Based on the electronic structure calculation, there is only one triplet state lower than the S_1 state in energy for each compound under S_1 geometry (see Table S4). The T_2 states are higher in energy than the S_1 state, and will unlikely be involved in the ISC and rISC processes. Therefore, the following ISC/rISC rate constants are calculated using eq 4 by taking only T_1 into account.

To investigate the transition character of S_1 and T_1 for these systems, we plot the frontier orbitals at S_1 and T_1 optimized geometries in Figure 3 for *m*-3CzBN, 4CzBN, and *o*-3CzBN

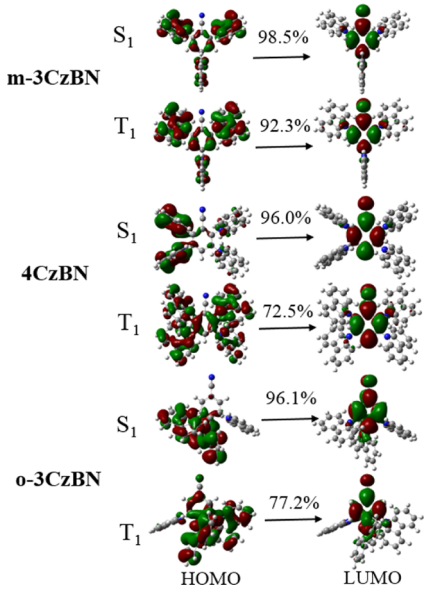

Figure 3. Frontier orbitals of S_1 and T_1 states under the PBEα_0/6−31+G* level for *m*-3CzBN, 4CzBN, and *o*-3CzBN.

and in Figure S2 for the remaining molecules. According to Figures 3 and S2, the main character of both S_1 and T_1 for all investigated systems is charge-transfer transition. Specifically, molecules with pure charge-transfer character such as Spiro-CN, DHPZ-2BTZ, PXZ-TRZ, 3-PXZ-XO, and DMAC-TRZ have almost zero ΔE_{ST} (Table 1) because of an almost complete spacial separation between HOMO and LUMO

https://dx.doi.org/10.1021/acs.jpca.0c09767
J. Phys. Chem. A 2021, 125, 1468−1475

Table 1. Comparison of the Adiabatic Energy Gap between S_1 and T_1($\Delta E_{ST\text{-}ad}$), Reorganization Energy (λ), ΔG_1, ΔG_2, and the Rate Constants of ISC and rISC[a]

energy/eV	$\Delta E_{ST\text{-}ad}$	λ	$\Delta G_{1\text{-}ISC}$	$\Delta G_{2\text{-}ISC}$	k_{ISC} (10^7 s^{-1})	$\Delta G_{1\text{-}rISC}$	$\Delta G_{2\text{-}rISC}$	k_{rISC} (10^6 s^{-1})
TADF-active								
4CzBN	0.23	0.23	~0	~0	3.43(57[c])	0.23	0.21	0.12(0.18[c])
4CzTPN	0.11	0.11	~0	~0	15.5	0.11	0.13	0.52
Spiro-CN	~0	~0	0.001	0.01	55.7(3.24[b])	0.0005	0.03(0.057[b])	64.3(0.005[b])
DHPZ-2BTZ	0.01	0.01	0.0001	0.02	32.2(4.9[d])	0.007	0.04(~0[b])	40.5(6.25[d])
PXZ-TRZ	0.01	0.01	2×10^{-5}	0.03	5.09	0.01	0.06	2.96
3-PXZ-XO	0.04	0.02	0.004	~0	22.3(0.88[c])	0.04	0.06	22.0(0.17[c])
DMAC-TRZ	0.01	0.01	~0	0.03	11.2(1.67[b])	0.01	0.06	4.32(0.80[b])
TADF-inactive								
2CzPN	0.18	0.82	0.05	0.05	0.05(2.1[c])	0.41	0.24	0.006(0.006[c])
o-3CzBN	0.23	1.14	0.18	0.14	0.009(4[c])	0.41	0.32	0.003(0[c])
2CzBN	0.22[e]	0.54	0.05	0.04	0.78(8[c])	0.27	0.23	0.0017(0[c])
m-3CzBN	0.24[e]	0.07	0.11	0.03	1.45(24[c])	0.35	0.21	0.0003(0[c])

[a]Experimental counterparts are shown in brackets. All of the energetics are given in the unit of eV. [b]Doped film. [c]Toluene solution. [d]Estimated from available experimental $\frac{\phi_{TADF}}{\phi_p} = 2{:}\ 1$ in the film. [e]Obtained via $\Delta E_{ST,ad} = \Delta E_{ST,00}(exp) - \Delta E_{ZPVE}$.

orbitals. For molecules with a subtle portion of local excitation character such as 4CzBN, 4CzTPN, 2CzPN, *o*-3CzBN, 2-CzBN, and *m*-3CzBN, ΔE_{ST} is slightly larger (~0.2 eV based on Table 1) due to the small but non-negligible overlap between the frontier orbitals. It can be seen from Table 1 that compounds with similar ΔE_{ST} values can be either TADF-active or -inactive. Therefore, we reinforce that ΔE_{ST} cannot be the appropriate descriptor of the TADF process.

According to eqs 8−10, the deformation of molecule between S_1 and T_1 also plays a role in the ISC and rISC processes. To explore the deformation between S_1 and T_1, we calculate λ between S_1 and T_1, and explicit numbers can be found in Table 1. It can be seen from Table 1 that for all TADF-active molecules, λ is very close in energy compared to $\Delta E_{ST\text{-}ad}$, while for TADF-inactive molecules, λ largely deviates from $\Delta E_{ST\text{-}ad}$, which consolidates that $\Delta E_{ST\text{-}ad} = \lambda$ is the optimal condition for TADF molecules.

Next, we analyze the main contribution of normal modes in reorganization energy between S_1 and T_1 in Figures 4 and S3. Results show that the contribution to the reorganization energy is mainly from low-frequency modes, especially the modes which change the dihedral angle between donor and acceptor, such as mode 9 (15.15 cm^{-1}), mode 14 (51.50 cm^{-1}) in *m*-3CzBN, mode 16 (58.14 cm^{-1}) in 4CzBN, and mode 18 (106.61 cm^{-1}) in *o*-3CzBN. Therefore, manipulating the dihedral angle between donor and acceptor is the key to control the reorganization energy between S_1 and T_1. This deformation between S_1 and T_1 has been experimentally explored via time-resolved infrared (TR-IR) spectroscopy.[19,20] Theoretically, we compute the IR spectra of S_0, S_1, and T_1 for all of the molecules and take the difference between S_1 (T_1) and S_0 to match the experimental TR-IR spectroscopy, as shown in Figure 5, for *m*-3CzBN, 4CzBN, and *o*-3CzBN, and

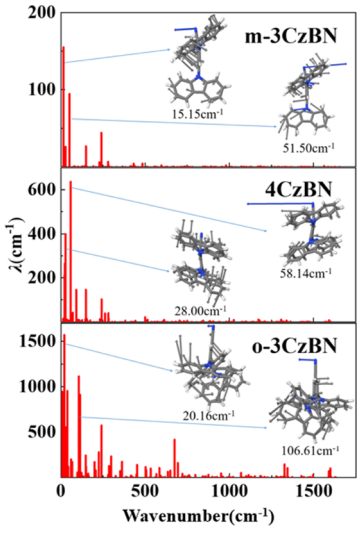

Figure 4. Reorganization energy and modes with mean contribution of *m*-3CzBN, 4CzBN, and *o*-3CzBN.

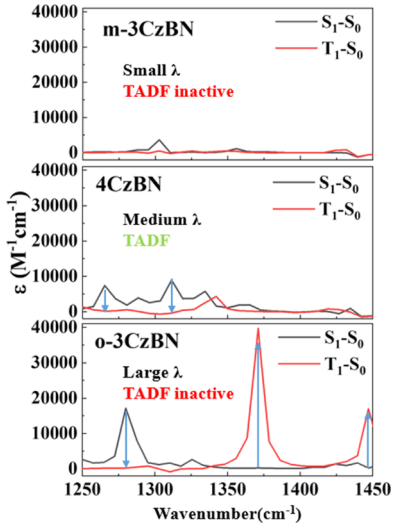

Figure 5. Differences between the vibrational profiles of S_1 and T_1 from that of S_0 for *m*-3CzBN, 4CzBN, and *o*-3CzBN, which can match experimental time-resolved infrared (TR-IR) spectroscopy.

Figure S4 for the remaining molecules. It is not hard to find that the molecule with a large λ tends to have significantly different TR-IR spectra for S_1 and T_1 (e.g., *o*-3CzBN). The large deformation of molecule gives rise to a large peak in the IR spectra. For molecules with little deformation between S_1

https://dx.doi.org/10.1021/acs.jpca.0c09767
J. Phys. Chem. A 2021, 125, 1468−1475

and T_1 (e.g., *m*-3CzBN), there is no obvious deviation in the TR-IR spectra for these two states.

The whole contribution from both ΔE_{ST} and λ can be gathered in ΔG, as indicated in eq 13. The calculated ΔG_{ISC} and ΔG_{rISC} values are listed in Table 1. Compared with the two available experimental results in Table 1, i.e., ΔG_{rISC} for Spiro-CN and DHPZ-2BTZ, the calculated values are in good agreement. To highlight the significance of ΔG, we plot the calculated rate constants (k_{ISC} and k_{rISC}) as a function of $\Delta G_{ISC/rISC}$ as well as ΔE_{ST} in Figure 6. For both k_{ISC} and k_{rISC},

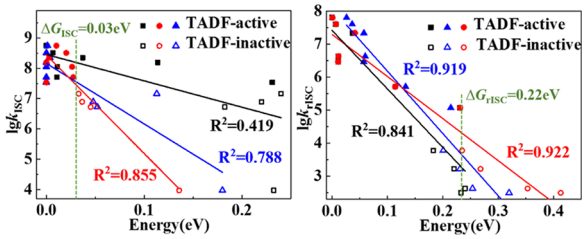

Figure 6. Relationship between ΔE_{ST} (black), ΔG_1 (blue), ΔG_2 (red), and the rate constant for ISC (left) and rISC (right) processes. Filled markers indicate TADF-active materials, and open markers indicate TADF-inactive materials. The solid lines are obtained from the linear fitting between ΔE_{ST}, ΔG_1, ΔG_2, and the rate constants. The green dashed lines indicate the threshold value of ΔG for TADF-active molecules among all investigated systems.

the linear fitting coefficient for both ΔG_1 and ΔG_2 is significantly larger than the 1 for ΔE_{ST}, indicating the fact that the ISC/rISC rate is more closely related to ΔG instead of ΔE_{ST}, as signified in Figure 1c. Specifically, the linear coefficients between the rate constants and ΔG_2 are even better than those between the rate constants and ΔG_1, since ΔG_2 is derived from a linear fitting between the temperature and the TVCF-calculated rate constant, in which the electron-vibration coupling effect has been explicitly taken into account. In addition, the kISC/rISC rate constants of the investigated systems obtained from real SOC are listed in Table S3, and the fluctuation of SOC is found to have no significant influence on the linear relationship between $k_{ISC/rISC}$ and ΔG.

It can be seen from Figure 6 that all TADF-active molecules (indicated by filled markers and listed in Table 1) have smaller ΔG values (blue triangle and red circle) compared to TADF-inactive counterparts for the ISC process, while the ΔE_{ST} (black square) values of these molecules are not necessarily smaller than those of TADF-inactive materials. Similar results can be obtained for the rISC process. Particularly, ΔE_{ST} is extremely close to ΔG for TADF-active molecules, which corresponds to the optimal case for efficient ISC and rISC processes, as indicated in Scheme 2. In addition, according to Figure 6, all TADF-active molecules have ΔG_{rISC} less than 0.22 eV and ΔG_{ISC} less than 0.03 eV, which can serve as a convenient criterion to screen out efficient TADF materials.

4. CONCLUSIONS

In this work, we have demonstrated that ΔG can serve as a more proper descriptor for TADF activity instead of the commonly used ΔE_{ST}. Eleven molecules with similar ΔE_{ST} (~0.2 eV) but different experimental TADF properties have been comprehensively investigated, and our results have shown that only molecules with small ΔG (i.e., when $\Delta E_{ST} \approx \lambda$) are TADF-active. A good linear relationship has been obtained between the ISC/rISC rate constant and ΔG, instead of ΔE_{ST}. Therefore, these molecules with smaller ΔG have larger ISC and rISC rates, which benefits TADF. Based on our analysis, $\lambda = \Delta E_{ST}$ is the condition when ΔG reaches its minimum, i.e., the most favorable situation for TADF phenomenon. Molecules with relatively large ΔG are not TADF-active even with an extremely small ΔE_{ST}. Practically, λ can be modified by manipulating the dihedral angle between D and A, making it possible to equal the value of ΔE_{ST}, which opens up a new direction in future TADF molecular design. The molecular descriptor ΔG is easy to implement, which would be very helpful for machine-learning-based research in the future.

■ ASSOCIATED CONTENT

Supporting Information

The Supporting Information is available free of charge at https://pubs.acs.org/doi/10.1021/acs.jpca.0c09767.

Scale factors of frequencies under cam-b3lyp/6-31g* level (Part 1); PBEα_0 method (Part 2); spin−orbit coupling constant of 11 molecule (Part 3); emission energy, ΔE_{ST}, with experimental counterparts and energy of T_2 (Part 4); Frontier orbitals (Part 5); reorganization energy (Part 6); TR-IR spectrum (Part 7); linear fit of Arrhenius equation to get ΔG_2 (Part 8); and T_1 geometry of UDFT and TDA, and *xyz* coordinates of all of the optimized geometries (Part 9) (PDF)

■ AUTHOR INFORMATION

Corresponding Authors

Qian Peng − *School of Chemical Sciences, University of Chinese Academy of Sciences, Beijing 100049, People's Republic of China;* orcid.org/0000-0001-8975-8413; Email: qpeng@iccas.ac.cn

Zhigang Shuai − *MOE Key Laboratory of Organic OptoElectronics and Molecular Engineering, Department of Chemistry, Tsinghua University, Beijing 100084, People's Republic of China;* orcid.org/0000-0003-3867-2331; Email: zgshuai@tsinghua.edu.cn

Authors

Lu Wang − *MOE Key Laboratory of Organic OptoElectronics and Molecular Engineering, Department of Chemistry, Tsinghua University, Beijing 100084, People's Republic of China*

Qi Ou − *MOE Key Laboratory of Organic OptoElectronics and Molecular Engineering, Department of Chemistry, Tsinghua University, Beijing 100084, People's Republic of China;* orcid.org/0000-0002-6400-7522

Complete contact information is available at: https://pubs.acs.org/10.1021/acs.jpca.0c09767

Notes

The authors declare no competing financial interest.

■ ACKNOWLEDGMENTS

This work was supported by the National Natural Science Foundation of China through the project "Science Center for Luminescence from Molecular Aggregates (SCELMA)," Grant No. 21788102, as well as by the Ministry of Science and Technology of China through the National Key R&D Plan,

Grant No. 2017YFA0204501. Q.O. is also supported by the Shuimu Tsinghua Scholar Program.

REFERENCES

(1) Uoyama, H.; Goushi, K.; Shizu, K.; Nomura, H.; Adachi, C. Highly efficient organic light-emitting diodes from delayed fluorescence. *Nature* **2012**, *492*, 234.
(2) Cao, X.; Zhang, D.; Zhang, S.; Tao, Y.; Huang, W. CN-Containing donor−acceptor-type small-molecule materials for thermally activated delayed fluorescence OLEDs. *J. Mater. Chem. C* **2017**, *5*, 7699−7714.
(3) Yang, Z.; Mao, Z.; Xie, Z.; Zhang, Y.; Liu, S.; Zhao, J.; Xu, J.; Chi, Z.; Aldred, M. P. Recent advances in organic thermally activated delayed fluorescence materials. *Chem. Soc. Rev.* **2017**, *46*, 915−1016.
(4) Bui, T. T.; Goubard, F.; Ibrahim-Ouali, M.; Gigmes, D.; Dumur, F. Recent advances on organic blue thermally activated delayed fluorescence (TADF) emitters for organic light-emitting diodes (OLEDs). *Beilstein J. Org. Chem.* **2018**, *14*, 282−308.
(5) Data, P.; Takeda, Y. Recent Advancements in and the Future of Organic Emitters: TADF- and RTP-Active Multifunctional Organic Materials. *Chem. - Asian J.* **2019**, *14*, 1613−1636.
(6) Godumala, M.; Choi, S.; Cho, M. J.; Choi, D. H. Recent breakthroughs in thermally activated delayed fluorescence organic light emitting diodes containing non-doped emitting layers. *J. Mater. Chem. C* **2019**, *7*, 2172−2198.
(7) Xue, C.; Lin, H.; Zhang, G.; Hu, Y.; Jiang, W.; Lang, J.; Wang, D.; Xing, G. Recent advances in thermally activated delayed fluorescence for white OLEDs applications. *J. Mater. Sci.: Mater. Electron.* **2020**, *31*, 4444−4462.
(8) Im, Y.; Kim, M.; Cho, Y. J.; Seo, J.-A.; Yook, K. S.; Lee, J. Y. Molecular Design Strategy of Organic Thermally Activated Delayed Fluorescence Emitters. *Chem. Mater.* **2017**, *29*, 1946−1963.
(9) Samanta, P. K.; Kim, D.; Coropceanu, V.; Brédas, J.-L. Up-Conversion Intersystem Crossing Rates in Organic Emitters for Thermally Activated Delayed Fluorescence: Impact of the Nature of Singlet vs Triplet Excited States. *J. Am. Chem. Soc.* **2017**, *139*, 4042−4051.
(10) Chen, X.-K.; Kim, D.; Brédas, J.-L. Thermally Activated Delayed Fluorescence (TADF) Path toward Efficient Electroluminescence in Purely Organic Materials: Molecular Level Insight. *Acc. Chem. Res.* **2018**, *51*, 2215−2224.
(11) Sanz-Rodrigo, J.; Olivier, Y.; Sancho-Garcia, J. C. Computational Studies of Molecular Materials for Unconventional Energy Conversion: The Challenge of Light Emission by Thermally Activated Delayed Fluorescence. *Molecules* **2020**, *25*, No. 1006.
(12) Walter, M. J.; Lupton, J. M. Spin Correlations in Organic Light-Emitting Diodes In *Highly Efficient OLEDs with Phosphorescent Materials*; Yersin, H., Ed.; Wiley-VCH Verlag GmbH & Co. KGaA, 2007; pp 99−129.
(13) Turro, N. J. *Modern Molecular Photochemistry*; Benjamin/Cummings Publ., 1978.
(14) Zhang, Q.; Li, J.; Shizu, K.; Huang, S.; Hirata, S.; Miyazaki, H.; Adachi, C. Design of efficient thermally activated delayed fluorescence materials for pure blue organic light emitting diodes. *J. Am. Chem. Soc.* **2012**, *134*, 14706−14709.
(15) Lee, J.; Shizu, K.; Tanaka, H.; Nakanotani, H.; Yasuda, T.; Kaji, H.; Adachi, C. Controlled emission colors and singlet−triplet energy gaps of dihydrophenazine-based thermally activated delayed fluorescence emitters. *J. Mater. Chem. C* **2015**, *3*, 2175−2181.
(16) Lower, S. K.; El-Sayed, M. A. The Triplet State and Molecular Electronic Processes in Organic Molecules. *Chem. Rev.* **1966**, *66*, 199−241.
(17) Peng, Q.; Niu, Y.; Shi, Q.; Gao, X.; Shuai, Z. Correlation Function Formalism for Triplet Excited State Decay: Combined Spin−Orbit and Nonadiabatic Couplings. *J. Chem. Theory Comput.* **2013**, *9*, 1132−1143.
(18) Peng, Q.; Fan, D.; Duan, R.; Yi, Y.; Niu, Y.; Wang, D.; Shuai, Z. Theoretical Study of Conversion and Decay Processes of Excited Triplet and Singlet States in a Thermally Activated Delayed Fluorescence Molecule. *J. Phys. Chem. C* **2017**, *121*, 13448−13456.
(19) Hosokai, T.; Matsuzaki, H.; Nakanotani, H.; Tokumaru, K.; Tsutsui, T.; Furube, A.; Nasu, K.; Nomura, H.; Yahiro, M.; Adachi, C. Evidence and mechanism of efficient thermally activated delayed fluorescence promoted by delocalized excited states. *Sci. Adv.* **2017**, *3*, No. e1603282.
(20) Saigo, M.; Miyata, K.; Tanaka, S.; Nakanotani, H.; Adachi, C.; Onda, K. Suppression of Structural Change upon S1-T1 Conversion Assists the Thermally Activated Delayed Fluorescence Process in Carbazole-Benzonitrile Derivatives. *J. Phys. Chem. Lett.* **2019**, *10*, 2475−2480.
(21) Chen, X.-K.; Zhang, S.-F.; Fan, J.-X.; Ren, A.-M. Nature of Highly Efficient Thermally Activated Delayed Fluorescence in Organic Light-Emitting Diode Emitters: Nonadiabatic Effect between Excited States. *J. Phys. Chem. C* **2015**, *119*, 9728−9733.
(22) Gibson, J.; Monkman, A. P.; Penfold, T. J. The Importance of Vibronic Coupling for Efficient Reverse Intersystem Crossing in Thermally Activated Delayed Fluorescence Molecules. *ChemPhysChem* **2016**, *17*, 2956−2961.
(23) Lv, L.; Yuan, K.; Zhao, T.; Wang, Y. A new mechanistic study of a second generation TADF material based on the path integral approach incorporating Herzberg−Teller and Duschinsky rotation effects. *J. Mater. Chem. C* **2020**, *8*, 10369−10381.
(24) Nakagawa, T.; Ku, S. Y.; Wong, K. T.; Adachi, C. Electroluminescence based on thermally activated delayed fluorescence generated by a spirobifluorene donor-acceptor structure. *Chem. Commun.* **2012**, *48*, 9580−9582.
(25) Tanaka, H.; Shizu, K.; Miyazaki, H.; Adachi, C. Efficient green thermally activated delayed fluorescence (TADF) from a phenoxazine−triphenyltriazine (PXZ−TRZ) derivative. *Chem. Commun.* **2012**, *48*, 11392−11394.
(26) Tsai, W. L.; Huang, M. H.; Lee, W. K.; Hsu, Y. J.; Pan, K. C.; Huang, Y. H.; Ting, H. C.; Sarma, M.; Ho, Y. Y.; Hu, H. C.; Chen, C. C.; Lee, M. T.; Wong, K. T.; Wu, C. C. A versatile thermally activated delayed fluorescence emitter for both highly efficient doped and non-doped organic light emitting devices. *Chem. Commun.* **2015**, *51*, 13662−13665.
(27) Zhang, Y.; Ma, H.; Wang, S.; Li, Z.; Ye, K.; Zhang, J.; Liu, Y.; Peng, Q.; Wang, Y. Supramolecular Structure-Dependent Thermally-Activated Delayed Fluorescence (TADF) Properties of Organic Polymorphs. *J. Mater. Chem. C* **2016**, *120*, 19759−19767.
(28) Lin, S. H.; Chang, C. H.; Liang, K. K.; Chang, R.; Shiu, Y. J.; Zhang, J. M.; Yang, T. S.; Hayashi, M.; Hsu, F. C. Ultrafast Dynamics and Spectroscopy of Bacterial Photosynthetic Reaction Centers. *Adv. Chem. Phys.* **2002**, 1−88.
(29) Alecu, I. M.; Zheng, J.; Zhao, Y.; Truhlar, D. G. Computational Thermochemistry: Scale Factor Databases and Scale Factors for Vibrational Frequencies Obtained from Electronic Model Chemistries. *J. Chem. Theory Comput.* **2010**, *6*, 2872−2887.
(30) Wang, C.; Deng, C.; Wang, D.; Zhang, Q. Prediction of Intramolecular Charge-Transfer Excitation for Thermally Activated Delayed Fluorescence Molecules from a Descriptor-Tuned Density Functional. *J. Phys. Chem. C* **2018**, *122*, 7816−7823.
(31) Marenich, A. V.; Cramer, C. J.; Truhlar, D. G. Universal Solvation Model Based on Solute Electron Density and on a Continuum Model of the Solvent Defined by the Bulk Dielectric Constant and Atomic Surface Tensions. *J. Phys. Chem. B* **2009**, *113*, 6378−6396.
(32) Frisch, M. J.; Trucks, G. W.; Schlegel, H. B.; Scuseria, G. E.; Robb, M. A.; Cheeseman, J. R.; Scalmani, G.; Barone, V.; Petersson, G. A.; Nakatsuji, H. et al. *Gaussian 16 Rev. C.01*; Wallingford, CT, 2016.
(33) Niu, Y.; Li, W.; Peng, Q.; Geng, H.; Yi, Y.; Wang, L.; Nan, G.; Wang, D.; Shuai, Z. MOlecular MAterials Property Prediction Package (MOMAP) 1.0: a software package for predicting the luminescent properties and mobility of organic functional materials. *Mol. Phys.* **2018**, *116*, 1078−1090.

https://dx.doi.org/10.1021/acs.jpca.0c09767
J. Phys. Chem. A 2021, 125, 1468−1475

(34) Niu, Y.; Peng, Q.; Shuai, Z. Promoting-mode free formalism for excited state radiationless decay process with Duschinsky rotation effect. *Sci. China, Ser. B: Chem.* **2008**, *51*, 1153−1158.
(35) Peng, Q.; Yi, Y.; Shuai, Z.; Shao, J. Toward Quantitative Prediction of Molecular Fluorescence Quantum Efficiency: Role of Duschinsky Rotation. *J. Am. Chem. Soc.* **2007**, *129*, 9333−9339.

https://dx.doi.org/10.1021/acs.jpca.0c09767
J. Phys. Chem. A 2021, 125, 1468−1475